Electronic Supporting Information (ESI)

Bi-underpotential/PtAu-bulk coelectrodeposition and subsequent Bi dissolution for electrocatalytic oxidation and amperometric analysis of formaldehyde

Yingying Chen,[a] Zhihui Qiao,[a] Huan Liu[a], Qingqing Yuan[a], Qingji Xie[a*] and Shouzhuo Yao[a,b]

[a]Key Laboratory of Chemical Biology and Traditional Chinese Medicine Research (MOE of China), National & Local Joint Engineering Laboratory for New Petro-chemical Materials and Fine Utilization of Resources, Hunan Normal University, Changsha 410081, China. E-mail: xieqj@hunnu.edu.cn

[b]State Key Laboratory of Chemo/Biosensing and Chemometrics, Hunan University, Changsha 410082, China

Contents

Experimental section

1. Instrumentation and reagents

All electrochemical experiments were conducted on a CHI660A electrochemical workstation (CH Instrument Co. USA). A conventional three-electrode system was employed in all electrochemical experiments. A disk glassy carbon electrode (GCE, 3 mm diameter), a KCl-saturated calomel electrode (SCE), and a platinum wire were employed as the working electrode, the reference electrode, and the counter electrodes, respectively. All potentials are reported with respect to SCE. Scanning electron microscopy (SEM) images and X-ray energy dispersive spectroscopy (EDS) were performed on a JEM-6700 field emission scanning electron microscope equipped with an EDS device. Quartz crystal microbalance (QCM) and electrochemical quartz crystal microbalance (EQCM) experiments were performed on the HP4395A impedance analyzer. We employed AT-cut 9 MHz piezoelectric quartz crystal (PQC, JA5B, Beijing Chenjing). The PQC wafer was fixed on one end of a plastic tube with silicone rubber (704, Wuxi, China), and only one PQC side faced the liquid solution. The geometric area of the PQC Au electrode is 0.14 cm^2.

$HAuCl_4 \cdot 4H_2O$, $H_2PtCl_6 \cdot 6H_2O$ and Bi_2O_3 were purchased from Tianjin Chemical Reagent Factory (Tianjin, China). HCHO, $K_4Fe(CN)_6 \cdot 3H_2O$, H_2SO_4, HCl, HNO_3, Nafion and commercial Pt/C (20%, weight percentage) were purchased from Sinopharm Group Chemical Reagent Co., Ltd. (Shanghai, China). Chemical reagents are of analytical grade or higher purity. Milli-Q ultrapure water (Millipore, 18 MΩ cm) was used throughout. All experiments were performed at room temperature (ca. 25 ^{o}C). The Bi_2O_3 solid was dissolved in concentrated $HClO_4$, and then diluted to the required concentration with ultrapure water. Aqua regia (V_{HCl}:V_{HNO3} = 3:1, highly corrosive, treat with great care) was used to dissolve Pt, Au and Bi.

2. Preparation and characterization of modified electrodes

The pretreatment of GCE was as follows. A GCE was polished with sandpapers and 0.05 μm alumina powder, rinsed with ultrapure water, and then ultrasonicated in ultrapure water, ethanol, and then ultrapure water each for 3 min. Subsequently, the GCE was treated with concentrated sulfuric acid for 15 s and then rinsed with ultrapure water, and this treatment was repeated three times. Afterwards, the GCE was placed in 0.5 M aqueous H_2SO_4 for electrochemical cleaning by cyclic voltammetry (CV, from -1.0~1.0 V, 50 mV s^{-1}) until the CV curves became reproducible. Finally, the GCE was placed in 0.1 M aqueous Na_2SO_4 containing 2.0 mM $K_4Fe(CN)_6$ for electrochemical characterization (from -0.1~0.5 V, 50 mV s^{-1}). The peak-to-peak separation (E_p) was around 75 mV (theoretically ca. 58 mV for a perfectly reversible one-electron electrode reaction on a disk electrode), showing that the GCE had been well cleaned.

For comparison, four different modified electrodes were prepared. (1) A $PtAu_{Bi\text{-}BD}$/GCE was prepared by potentiostatic deposition on a GCE at the potential of Bi BD (-0.04 V vs SCE) for 300 s in magnetically stirred (1000 rpm) aqueous 0.5 M $HClO_4$ + 7.0 mM H_2PtCl_6 + 3.0 mM $HAuCl_4$ + 100 mM Bi(III), followed by the acid treatment of Bi similar to the $PtAu_{Bi\text{-}UPD}$/GCE case. (2)-(3): A $PtAu_{-0.04V}$/GCE and a $PtAu_{0V}$/GCE were prepared for 300 s on a GCE in 0.5 M aqueous $HClO_4$ containing 7.0 mM H_2PtCl_6 and 3.0 mM $HAuCl_4$ by potentiostatic deposition at -0.04 V and 0 V, respectively. (4) A Pt/C/Au_{pla}/GCE was prepared as follows. 0.5 mg commercial Pt/C catalyst (Pt on C, 20% w/w Pt) was added in 1 mL ultrapure water for 1 h ultrasonic dispersion, and 10 μL of the suspension was then cast-coated on an Au_{pla}/GCE and dried at room temperature. Afterwards, 4 μL Nafion ethanol solution (0.5 wt.%) was cast-coated on the electrode surface and dried at room temperature. All the modified electrodes were characterized by CV in 0.5 M aqueous H_2SO_4 until the CV curves became reproducible (from -0.3~1.45 V, 50 mV s^{-1}).

3. Electrocatalytic experiments

The electrocatalytic oxidation of formaldehyde was conducted by CV (from -0.2~0.9 V, 50 mV s^{-1}) in 0.5 M aqueous H_2SO_4 containing 0.1 M HCHO. The stability of the modified electrode for the catalytic oxidation of formaldehyde was investigated by the *i*-*t* method. The amperometric detection of formaldehyde carried out in 0.5 M aqueous H_2SO_4 by chronoamperometry at 0.7 V.

QCM estimation of the mass of stripped Bi atoms

The mass changes (Δm) and the corresponding frequency changes (Δf_0) on QCM Au electrode should obey the Sauerbrey equation[1], $\Delta f_0 = (-2.264\times10^{-6}\times f_{0g}^{2}\times\Delta m)/A$, where f_{0g} (9 MHz) is the fundamental frequency in air, and A (0.14 cm^2 here) is the piezoelectric active area of the electrode. Thus, the mass of Bi atoms stripped (Δf_0 = -52 kHz) is calculated to be $-52000\times0.14/(-2.264\times10^{-6}\times(9\times10^{6})^{2}) = 39.7$ μg.

Table S1. Component analysis of Pt, Au and Bi on modified electrodes by electrochemical method

Electrode	Test element	Constant volume (μL)	Detected (μg)	Added (μg)	Found (μg)	RSD[a] (%)	Recovery (%)	Sample element content (w%, weight percentage)
A*	Pt	50	258	250	526	3.2	107	57.1
	Au	50	126	120	252	4.5	105	27.9
	Bi	50	67.4	60.0	123	6.3	92.7	14.9
B*	Pt	50	247	250	511	2.9	106	68.0
	Au	50	113	120	241	4.2	107	31.0
	Bi	50	3.46	5.00	8.72	7.2	105	0.95

*A: $PtAu_{Bi\text{-}UPD0}$/GCE; B: $PtAu_{Bi\text{-}UPD}$/GCE.

Component analysis of Pt, Au and Bi of $PtAu_{Bi\text{-}UPD0}$/GCE and $PtAu_{Bi\text{-}UPD}$/GCE was conducted by CV or linear sweep ASV (LSASV) and the standard addition method. In order to ensure the reliability of the material composition, thirty modified electrodes were prepared in parallel under the same conditions, and the metal material on the electrode surface were scraped off and collected in a centrifuge tube for weighing the mass. After dissolving some scraped $PtAu_{Bi\text{-}UPD0}$ or $PtAu_{Bi\text{-}UPD}$ with 40 μL aqua regia (V_{HCl}:V_{HNO3} = 3:1, highly corrosive, treat with great care), then adding 10 μL of 1 M aqueous HCl or 10 μL of 1 M aqueous HCl containing $PtCl_6^{2-}$, $AuCl_4^-$ and Bi(III) with known standard concentration (Table S1), CV or LSASV experiment was conducted on GCE. Due to the proportional relation of electric charge (Q) with concentration (c) of a metal component in the detection solution ($c_{detected}/Q_{detected} = c_{total}/Q_{total}$), the mass ($m$) of Pt, Au or Bi on $PtAu_{Bi\text{-}UPD0}$/GCE and $PtAu_{Bi\text{-}UPD}$/GCE can be estimated as follows: $m_{detected}/Q_{detected} = (m_{detected} + m_{standard})/Q_{total}$ (also see Fig. S7, with discussion detailed).

Table S2. Component analysis of Pt, Au and Bi on modified electrodes by ICP-AES*

Sample	Test element	Sample element content (mg/g)	Sample element content (w%, weight percentage)
$PtAu_{Bi\text{-}UPD0}$	Pt	530	53
	Au	250	25
	Bi	171	17.1
$PtAu_{Bi\text{-}UPD}$	Pt	650	65
	Au	300	30
	Bi	9.6	0.96

*In order to ensure the reliability of the ICP-AES measurement of the material composition, thirty modified electrodes were prepared in parallel under the same conditions, and the metal material on the electrode surface were scraped off and collected in a centrifuge tube for weighing the mass, fully dissolved the collected metal materials with 1 mL of freshly prepared aqua regia (3:1, V_{HCl}/V_{HNO3}, highly corrosive, treat with great care), and finally diluted the total volume of the dissolved solution to 10 mL with ultrapure water. The diluted solution was drawn into the ICP-AES instrument, and the material composition was determined by the standard curve method. Therefore, the element content on the relevant modified electrode can be calculated from the solution volume and concentration.

Table S3. Performance comparison among different amperometric HCHO sensors

Type of materials or electrode	LDR (mM)	Sensitivity (μA mM^{-1} cm^{-2})	LOD (μM)	Applied potential (V vs. SCE when not specified)	Medium	Reference
Fe@Pt NPs	0.0125-15.4	40.2	3.75	0.4	PB (0.1 M, pH 7.0)	2
PtAuPd/IL	0.05-28	50.3	-	0.5	H_2SO_4 (0.2 M)	3
Platinized gold electrodes	0.02-2	2818	50	0 V vs Ag/AgCl	PB (20 mM, pH 7.0)	4
Pt/EG/GCE	0-2	231	40	0.35 V vs Ag/AgCl	H_2SO_4 (1 M)	5
Pt-Pd/Nf/GCE	0.01-1	-	3	0.58	H_2SO_4 (0.1 M)	6
Pd_2Pt_1-PPy /N-rGO NC/GCE	0.01-0.9	346	27	0.55	H_2SO_4 (0.1 M)	7
Pd NW/GCE	0.002-1	1360	0.5	0.05 V vs Ag/AgCl	KOH (0.1 M)	8
AgPd/Ch-IL/GCE	0.06-20	0.043	22	0.05	NaOH (0.1 M)	9
Pd/TiO_2	0-17.7	207	15	-0.4 V vs Ag/AgCl	NaOH (0.1 M)	10
Au/PPy/GCE	0.4-2.4	-	20	-0.5	NaOH (1 M)	11
$PtAu_{Bi\text{-}UPD}$/GCE	0.005-33	1720	5	0.7	H_2SO_4 (0.5 M)	This work

NPs: nanoparticles; PB: phosphate buffer; IL: ionic liquid; EG: electrodeposited graphene; Nf: Nafion; PPy: polypyrrole; N-rGO: nitrogen-doped reduced graphene oxide; NC: nanocomposites; NW: nanowire; Ch: chitosan.

Table S4. Determination of formaldehyde in a real sample with $PtAu_{Bi\text{-}UPD}/GCE$

Sample	Dilution fold	Detected (mM)	Added (mM)	Found (mM)	RSD[a] (%)	Recovery (%)
Wallpaper basilemma	2	0.0143	0.0150	0.0286	3.3	95
	3	0.0954	0.0100	0.0191	3.1	96
	4	0.00711	0.00700	0.0144	4.3	104

[a] RSD (Relative standard deviation): obtained from 3 determinations.

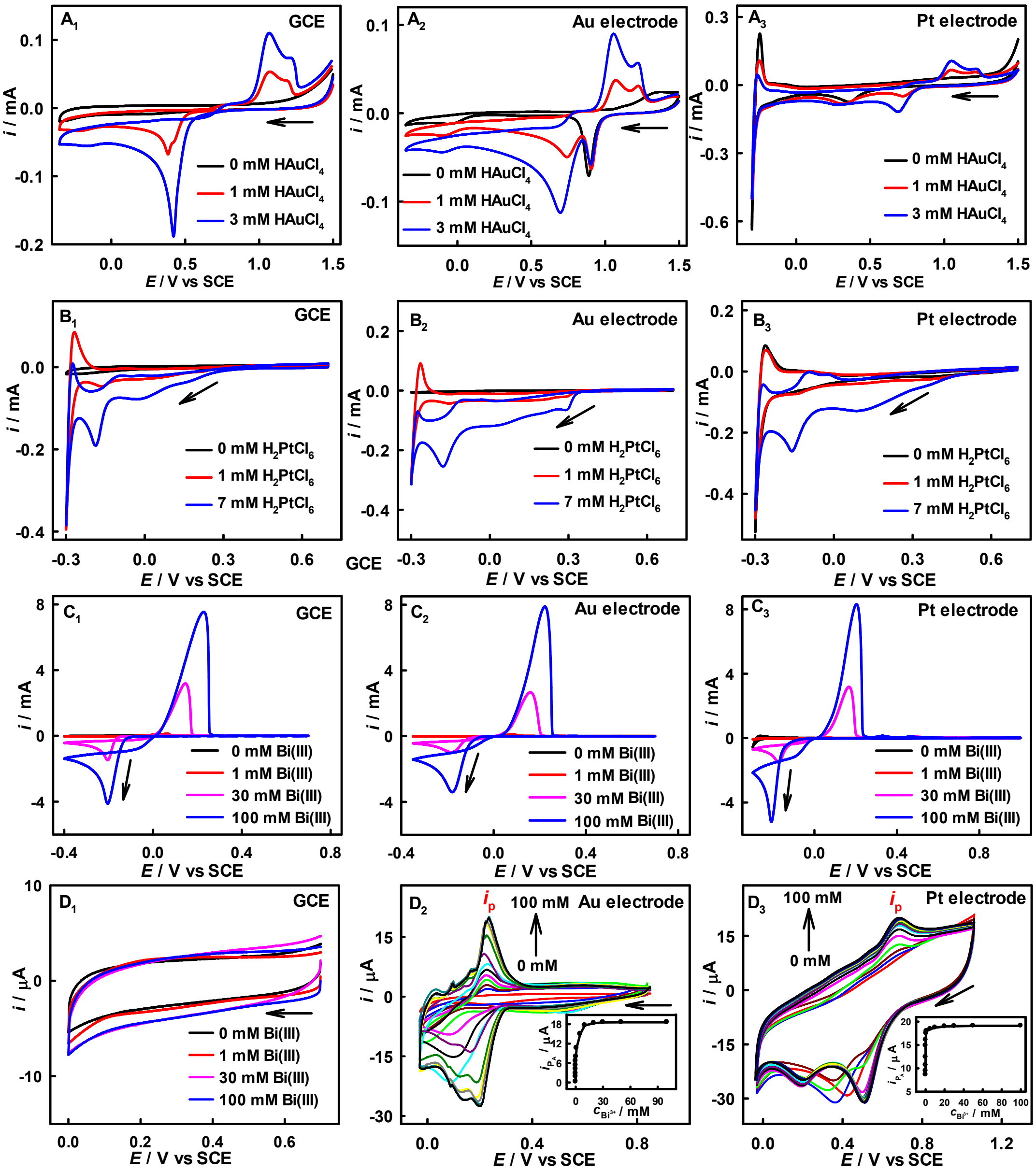

Fig. S1. CV curves on GCE (A_1), Au (A_2) or Pt (A_3) disk electrodes in 0.5 M aqueous $HClO_4$ containing $HAuCl_4$ at different concentrations (0, 1 or 3 mM). CV curves on GCE (B_1), Au (B_2) or Pt (B_3) disk electrodes in 0.5 M aqueous $HClO_4$ containing H_2PtCl_6 at different concentrations (0, 1 or 7 mM). CV curves on GCE (C_1 and D_1), Au (C_2) or Pt (C_3) disk electrodes in 0.5 M aqueous $HClO_4$ containing Bi(III) at different concentrations (0, 1, 30 or 100 mM). CV curves on Au (D_2) or Pt (D_3) disk electrodes in 0.5 M aqueous $HClO_4$

containing Bi(III) at different concentrations (0, 0.001, 0.005, 0.01, 0.05, 0.1, 0.5, 1, 5, 10, 20, 30, 50 and 100 mM). Scan rate: 50 mV s^{-1}.

Figure Note: The preparation of the modified electrode involves the UPD of Bi and the BD of Pt and Au. We thus investigated the electrochemical behavior of aqueous $HAuCl_4$, H_2PtCl_6, or Bi(III) on GCE, or Au and Pt electrodes by CV. As shown in Fig. S1A_1, the bare GCE showed almost no redox peaks in $HAuCl_4$-free 0.5 M aqueous $HClO_4$, and the oxidation current ramp due to oxygen evolution appeared at potentials positive than ca. 1.3 V. In 0.5 M aqueous $HClO_4$ containing 1 or 3 mM $HAuCl_4$, the reduction peaks at ca. 0.45 V and ca. -0.1 V can be assigned to the reduction of $AuCl_4^-$ on GCE and the reduction of oxygen at the active site of deposited gold, respectively, and the oxidation peaks near ca. 1.2 V are due to the electrooxidation of Au. The redox peak signals were higher in the 3 mM $HAuCl_4$ case (versus the 1 mM $HAuCl_4$ case). As shown in Fig. S1A_2, in $HAuCl_4$-free 0.5 M aqueous $HClO_4$, the Au electrode exhibited its characteristic redox peaks (anodic peaks at ca. 1.3 V for the formation of gold oxides (AuO_x) and a cathodic peak at ca. 0.88 V for the reduction of AuO_x) and the reduction peak of dissolved oxygen at ca. -0.1 V[12]. In 0.5 M aqueous $HClO_4$ containing 1 or 3 mM $HAuCl_4$, in addition to the reduction peaks of Au substrate electrode and dissolved oxygen, the reduction peak of ca. 0.7 V corresponds to the reduction of $AuCl_4^-$ on the Au electrode, and the oxidation peaks of ca. 1.2 V are attributed to the oxidation of electrodeposited Au. The redox peak signals were higher in the 3 mM $HAuCl_4$ case (versus the 1 mM $HAuCl_4$ case). As shown in Fig. S1A_3, in $HAuCl_4$-free 0.5 M aqueous $HClO_4$, the Pt electrode exhibited its characteristic electrochemical behavior (cathodic peak at ca. 0.35 V for the reduction of platinum oxide (PtO_y) and the dissolved oxygen in the solution, the redox peaks between -0.28 V and 0 V for the adsorption and desorption of atomic hydrogen on the Pt surface, a sharp current ramp appeared at -0.3 V for hydrogen evolution on the Pt surface, and the oxidation current ramp between 1.3 V and 1.5 V for oxygen evolution on Pt electrode[13]). In 0.5 M aqueous $HClO_4$ containing 1 or 3 mM $HAuCl_4$, in addition to the characteristic peaks of the Pt electrode, the reduction peak at ca. 0.7 V and the oxidation peaks of ca. 1.2 V are due to the reduction of $AuCl_4^-$ and the oxidation of Au on the Pt electrode, respectively. The Au-based redox peak signals were higher in the 3 mM $HAuCl_4$ case (versus the 1 mM $HAuCl_4$ case). Due to the partial occupation of the Pt sites by electrodeposited Au, the characteristic peaks of Pt decreased with the increase of $HAuCl_4$ concentration. The reduction peak potentials of $AuCl_4^-$ on Au and Pt electrodes are more positive than that on GCE, indicating the Au-Au or Au-Pt affinity stronger than the Au-C one. In summary, the BD of Au can occur here on GCE, and Au and Pt electrodes at potentials negative than ca. 0.6 V.

As shown in Fig. S1B_1 and S1B_2, the bare GCE/Au electrode showed almost no redox peaks in H_2PtCl_6-free 0.5 M aqueous $HClO_4$. In 0.5 M aqueous $HClO_4$ containing 1 or 7 mM H_2PtCl_6, the reduction peaks from -0.2 V to 0.3 V and the ramp current at -0.3 V on GCE and Au electrode correspond to the reduction of $PtCl_6^{2-}$ and hydrogen evolution at the deposited Pt, respectively. The oxidation peaks from -0.2 V to 0 V are due to the desorption of H atoms on the active sites of deposited platinum. The Pt-based redox peak signals were higher in the 7 mM H_2PtCl_6 case (versus the 1 mM H_2PtCl_6 case). In 0.5 M aqueous $HClO_4$ containing 1 or 7 mM H_2PtCl_6, the reduction peaks from -0.2 V to 0.4 V and the ramp current at -0.3 V are ascribed to $PtCl_6^{2-}$ reduction on the Pt electrode and hydrogen evolution on the Pt surface, and the oxidation peak from -0.2 V to 0 V are due to the desorption of H atoms on Pt. The Pt-based redox peak signals were higher in the 7 mM H_2PtCl_6 case (versus the 1 mM H_2PtCl_6 case). In addition, as shown in Fig. S1B$_1$-B$_3$, with the increase of H_2PtCl_6 concentration, the H-desorption current ramp from -0.3 V to -0.24 V and the H-desorption current plateau from -0.2 V to 0 V decreased, which is due to the reduction of $PtCl_6^{2-}$ in the solution. In summary, the BD of Pt can occur here on GCE, and Au and Pt electrodes at potential more negative than ca. 0.3 V.

As shown in Fig. S1C$_1$-C$_3$, the bare Au/GCE showed almost no redox peaks and the Pt electrode exhibited the characteristic electrochemical behavior of Pt in H_2PtCl_6-free 0.5 M aqueous $HClO_4$. In 0.5 M aqueous $HClO_4$ containing 1, 30 or 100 mM Bi(III), the reduction peak at ca. -0.2 V corresponds to the bulk reduction of Bi(III) on GCE, and Au and Pt electrodes, the oxidation peak at ca. 0.15 V is attributed to the electrooxidation of Bi. The Bi-based redox peak signals were increased with the concentration increase of Bi(III) concentration.

As shown in Fig. S1D$_1$, the bare GCE shows almost no redox peaks in 0.5 M aqueous $HClO_4$ containing 1, 30 or 100 mM Bi(III), indicating the failure of Bi UPD directly on GCE, as expected. As shown in Fig. S1D$_2$ for Au electrode and 0.5 M aqueous $HClO_4$ containing Bi(III) at a concentration from 0.001 to 100 mM, the redox peaks for Bi UPD and anodic stripping of UPD Bi appeared at potentials near 0.3 V. As shown in Fig. S1D$_3$ for Pt electrode and 0.5 M aqueous $HClO_4$ containing Bi(III) at a concentration from 0.001 to 100 mM, the reduction peak of PtO_y and the dissolved oxygen in the solution was split into two reduction peaks, probably due to the partial occupation of UPD Bi atoms on the Pt sites. The oxidation peak at ca. 0.6 V is due to the electrooxidation of UPD Bi. The bismuth-related signals were intensified with the increase of Bi(III) concentration and became almost unchanged when the Bi(III) concentration was 30 mM or larger, as reported previously for the UPD of Bi on Au electrode[14]. In order to achieve the largest intervention effect of UPD, the Bi(III) concentration should be significantly higher than that of H_2PtCl_6 and $HAuCl_4$. Taking the above factors into consideration, 100 mM was chosen as the concentration of Bi(III).

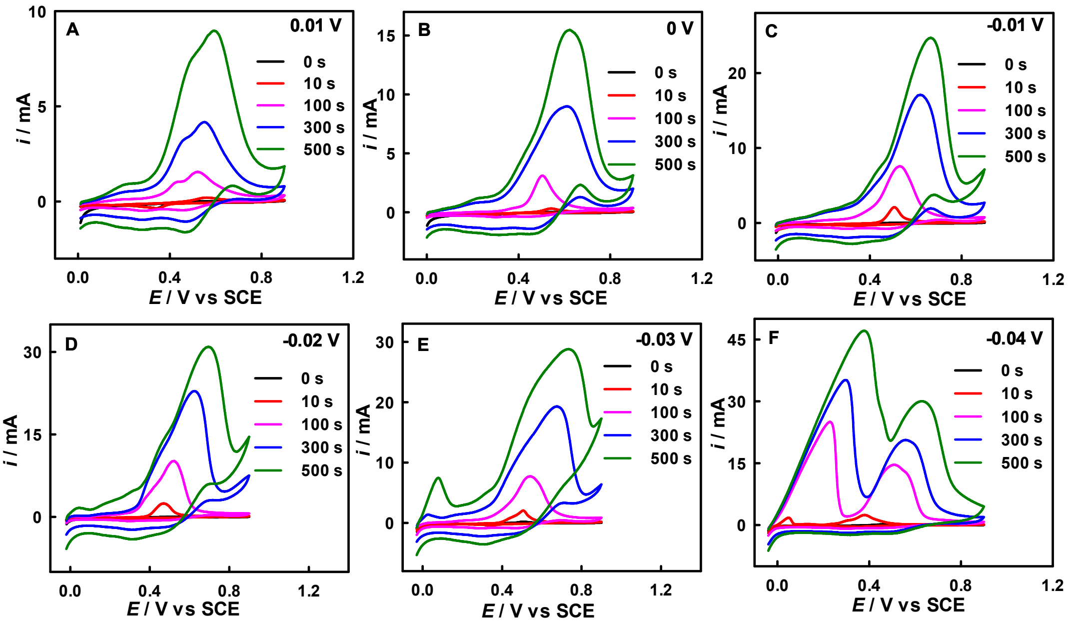

Fig. S2. CV curves on GCE after electrodeposition in 7.0 mM H_2PtCl_6 + 3.0 mM $HAuCl_4$ + 0.1 M Bi(III) + 0.5 M $HClO_4$ solution at different potentials (A: 0.01 V, B: 0 V, C: -0.01 V, D: -0.02 V, E: -0.03 V, F: -0.04 V) for different time (0 s, 10 s, 100 s, 300 s or 500 s). Scan rate: 50 mV s^{-1}. Here, in order to optimize the optimal deposition potential for UPD interventions, we performed CV and linear sweep anode stripping voltammetry (LSASV) experiments on GCE. As shown in Fig. S2, the negative potential terminal set from -0.01 to 0.01 V for preconcentration even for 500 s returned only the UPD-Bi anodic stripping peak at ca. 0.6 V, and the more negative preconcentration potential (-0.01 ~ 0.01 V) gave the larger peak response. In contrast, the negative potential terminal set from -0.04 to -0.02 V returned both the BD-Bi anodic stripping peak at ca. 0 V (increased with the negative shift of potential) and the UPD-Bi anodic stripping peak at ca. 0.6 V (changed little with the negative shift of potential). In summary, the BD of Bi cannot occur at 0 V under the experimental conditions.

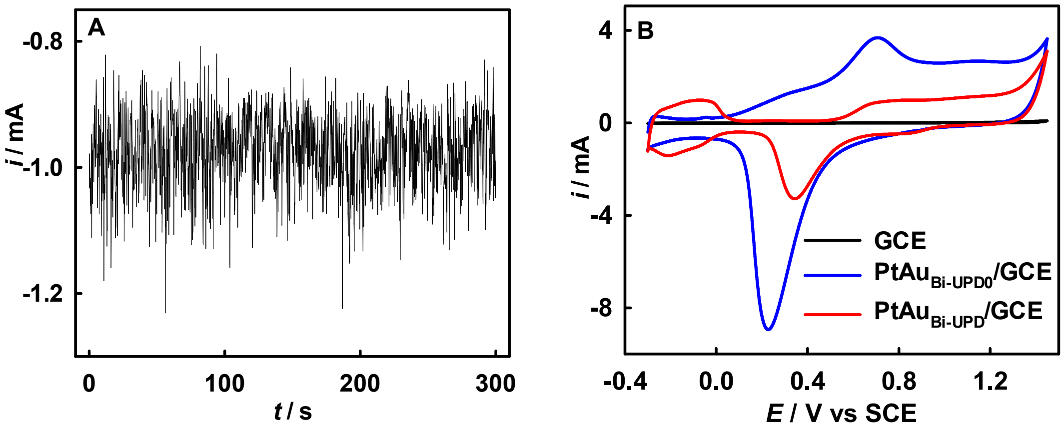

Fig. S3. (A) Chronoamperometric curve on GCE at 0 V for 300 s in stirred 7.0 mM H_2PtCl_6 + 3.0 mM $HAuCl_4$ + 0.1 M Bi(III) + 0.5 M $HClO_4$ solution. (B) CV curves on GCE, PtAu$_{Bi-UPD0}$/GCE and PtAu$_{Bi-UPD}$/GCE in 0.5 M aqueous H_2SO_4. Scan rate: 50 mV s^{-1}. Here, the preparation of the target electrode briefly includes two following steps: (i) Bi-underpotential/PtAu-bulk codeposition on a GCE to prepare a PtAu$_{Bi-UPD0}$/GCE; (ii) Concentrated HNO_3 dissolution of Bi to prepare the PtAu$_{Bi-UPD}$/GCE. In the first step, a PtAu$_{Bi-UPD0}$/GCE was potentiostatically prepared by Bi-underpotential/PtAu-bulk codeposition on a GCE at the potential of Bi UPD (0 V vs SCE) for 300 s in magnetically stirred (1000 rpm) aqueous 0.5 M $HClO_4$ + 7.0 mM H_2PtCl_6 + 3.0 mM $HAuCl_4$ + 100 mM Bi(III), as shown in Fig. S3A. The larger cathodic currents imply the cathodic deposition of atomic Pt, Au and Bi. As shown in Fig. S3B, the bare GCE shows almost no redox peaks. The oxidation peak of PtAu$_{Bi-UPD0}$/GCE at ca. 0.6 V is due to the electrooxidation of UPD Bi. The oxidation peak of Pt partially overlaps with the anodic stripping peak of Bi. The reduction peak at ca. 0.3 V is mainly attributed to the reduction of Bi(III) (UPD) and PtO_y. The PtAu$_{Bi-UPD}$/GCE shows characteristic electrochemical behavior for Au and Pt (anodic current platform from 0.6 V to 1.3 V for the formation of AuO_x and PtO_y, cathodic peak at ca. 0.88 V for the reduction of AuO_x, cathodic peak at ca. 0.45 V for the reduction of PtO_y and the dissolved oxygen in the solution, the redox peaks between -0.28 V and 0 V for the adsorption and desorption of atomic hydrogen on the Pt surface, a sharp current ramp appeared at -0.3 V for the hydrogen evolution on the Pt surface, the oxidation current ramp from 1.3 V to 1.45 V for oxygen evolution).

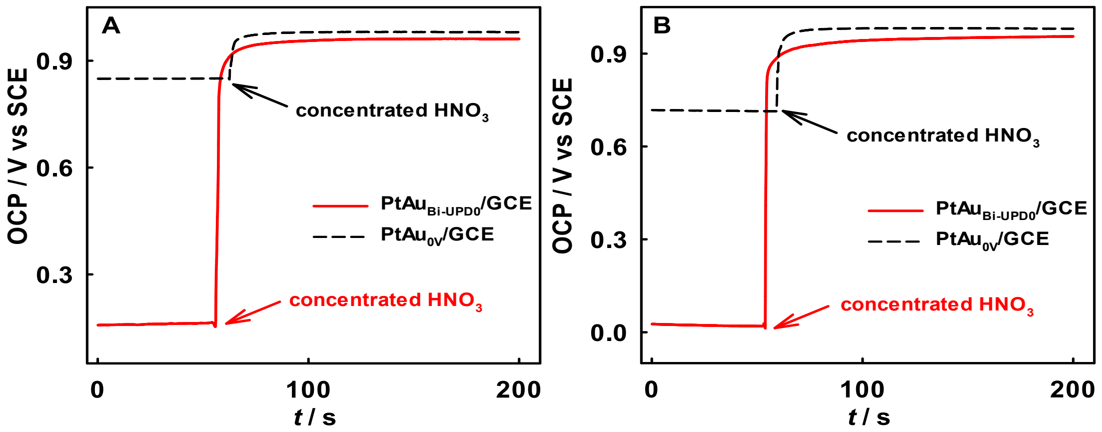

Fig. S4. The OCP-time curve on PtAu$_{\text{Bi-UPD0}}$/GCE and PtAu$_{\text{0V}}$/GCE to the addition of concentrated HNO$_3$ into stirred 0.5 M aqueous HNO$_3$ (A) or NaNO$_3$ (B). Here, in the second step, a PtAu$_{\text{Bi-UPD0}}$/GCE was treated with concentrated HNO$_3$ for 10 s and then rinsed with ultrapure water, and this treatment was repeated three times to obtain PtAu$_{\text{Bi-UPD}}$/GCE. The open circuit potential (OCP)-time curves are shown in Fig. S4. The OCP of PtAu$_{\text{Bi-UPD0}}$/GCE and PtAu$_{\text{0V}}$/GCE in 0.5 M aqueous HNO$_3$ were ca. 0.16 V and 0.85 V, respectively. The OCP of PtAu$_{\text{Bi-UPD0}}$/GCE and PtAu$_{\text{0V}}$/GCE in 0.5 M aqueous NaNO$_3$ were 0 V and 0.7 V, respectively. After adding excessive concentrated HNO$_3$, the OCP of PtAu$_{\text{Bi-UPD0}}$/GCE and PtAu$_{\text{0V}}$/GCE both rapidly increased to ca. 0.96 V. The former is mainly attributed to the oxidation of Bi by concentrated HNO$_3$, and the latter is mainly attributed to the sharp decrease of the pH after the addition of concentrated HNO$_3$. In summary, a large number of Pt and Au active sites were exposed after the acid dissolution of Bi, indicating that the PtAu$_{\text{Bi-UPD}}$/GCE was successfully prepared.

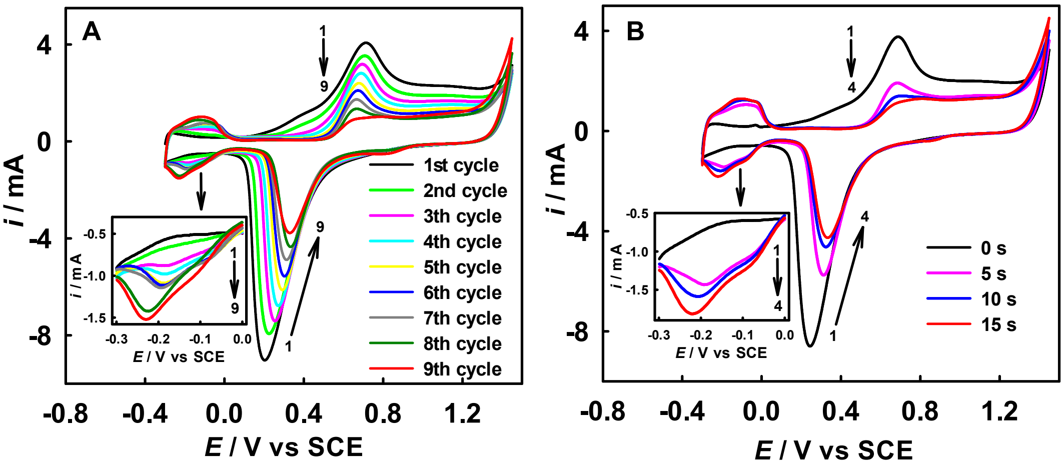

Fig. S5. (A) CV curves on PtAu$_{\mathrm{Bi\text{-}UPD0}}$/GCE in 0.5 M aqueous H_2SO_4. (B) CV curves on PtAu$_{\mathrm{Bi\text{-}UPD0}}$/GCE in 0.5 M aqueous H_2SO_4 after stripping of Bi by concentrated HNO_3 for 0 s, 5 s, 10 s or 15 s. Scan rate: 50 mV s^{-1}. As shown in Fig. S5A, the redox peaks of bismuth decreased cycle by cycle, due to the anodic stripping of atomic Bi from the electrode surface and somewhat cathodic re-deposition resulting from the diffusion of Bi(III) toward the bulk solution. At the same time, the reduction peaks of AuO_x/PtO_y and the absorption/desorption peaks of H increased cycle by cycle. As shown in Fig. S5B, with the increase of the stripping time of atomic Bi by concentrated HNO_3, the redox peaks of bismuth decreased, the reduction peaks of AuO_x/PtO_y, and the absorption/desorption peaks of H increased gradually. Due to the rapidness and convenience, we chose the stripping of Bi by concentrated HNO_3.

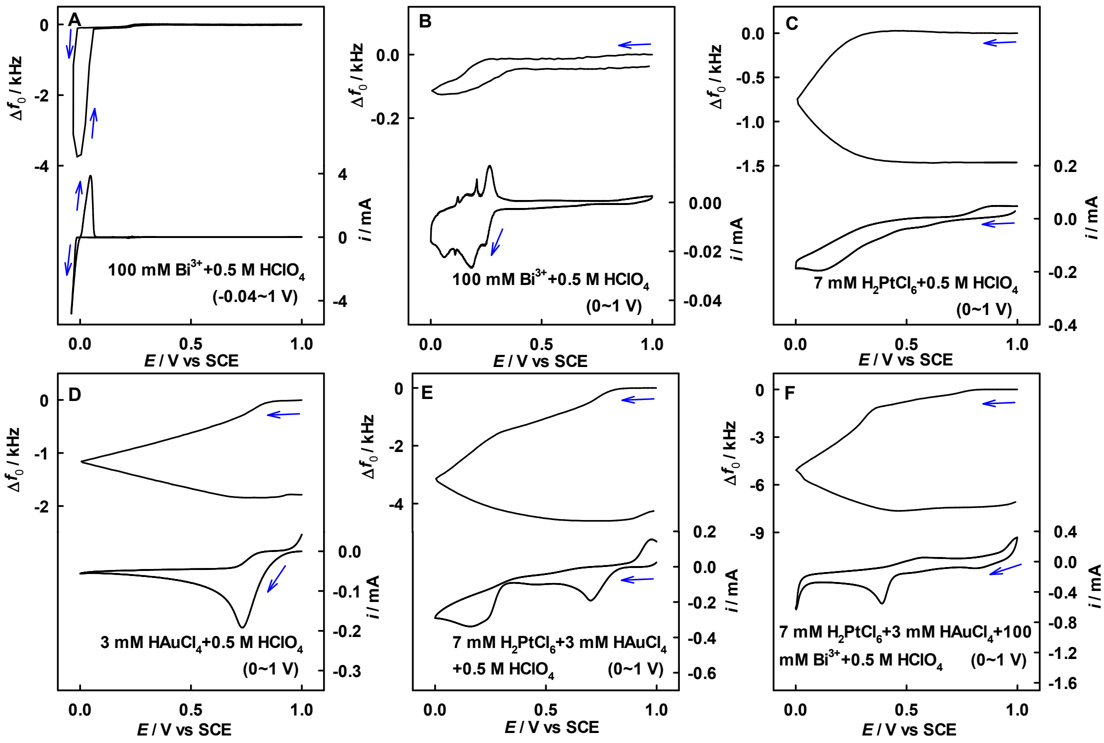

Fig. S6. Simultaneous responses of current and frequency changes (Δf_0) on bare QCM Au electrode during potential cycling in 100 mM Bi(III) + 0.5 M $HClO_4$ (A and B), 7.0 mM H_2PtCl_6 + 0.5 M $HClO_4$ (C), 3.0 mM $HAuCl_4$ + 0.5 M $HClO_4$ (D), 7.0 mM H_2PtCl_6 + 3.0 mM $HAuCl_4$ + 0.5 M $HClO_4$ (E) or 7.0 mM H_2PtCl_6 + 3.0 mM $HAuCl_4$ + 100 mM Bi(III) + 0.5 M $HClO_4$ (F). A: -0.04~1 V; B-F: 0~1 V. Scan rate: 30 mV s^{-1}. As shown in Fig. S6A, during the negative sweep of the potential, a reduction current ramp appeared from -0.04 to -0.02 V, and a significant decrease in frequency was observed, proving that the BD of Bi occurred on the QCM Au electrode. An oxidation peak appeared at 0 V, and a significant frequency increase was simultaneously observed, indicating the anodic stripping of BD Bi atoms. As shown in Fig. S6B, on the negative potential sweep, the Bi-UPD peaks appeared from 0.3 to 0 V and the frequency simultaneously decreased, proving the UPD of Bi on QCM Au electrode. On positive potential sweep, oxidation peaks appeared from 0 to 0.3 V and the frequency simultaneously increased, indicating the anodic stripping of UPD Bi atoms. As shown in Fig.

S6C, on the negative potential sweep, a reduction peak appeared from ca. 0.4 to 0 V, with a simultaneous decrease in frequency, indicating the occurrence of Pt BD on QCM Au electrode. On the positive potential sweep, the frequency decreased from 0 to 0.3 V due to continuous Pt BD; the oxidation current plateau at ca. 0.8 V is attributed to the surface oxidation of Pt and substrate Au, where the frequency change should be very small in principle. As shown in Fig. S6D for the absence of Bi(III), the cathodic currents due to the BD of Au and Pt were accompanied with the notable decrease in frequency, and the anodic currents due to the surface oxidation of deposited Pt and Au gave the much smaller frequency response. As shown in Fig. S6E for the presence of Bi(III), during the negative sweep of the potential, two reduction peaks appeared with a decrease in frequency, proving that Au and Pt BD occurred on the surface of the QCM Au electrode. During the positive sweep of the potential, the frequency decreases from 0 to 0.7 V was attributed to Au and BD; the oxidation current plateau and oxidation current ramp appeared from 0.8 to 1 V and the frequency increased, which is attributed to the oxidation of Au and Pt. As shown in Fig. S6F, on the negative potential sweep, the currents for the BD of Au and Pt and the UPD of Bi were accompanied with frequency decrease larger than that in Fig. S6E. On the positive potential sweep, an oxidation peak for anodic stripping of UPD Bi appeared at ca. 0.6 V, and a slow increase in frequency was simultaneously observed, indicating the anodic stripping of UPD Bi.

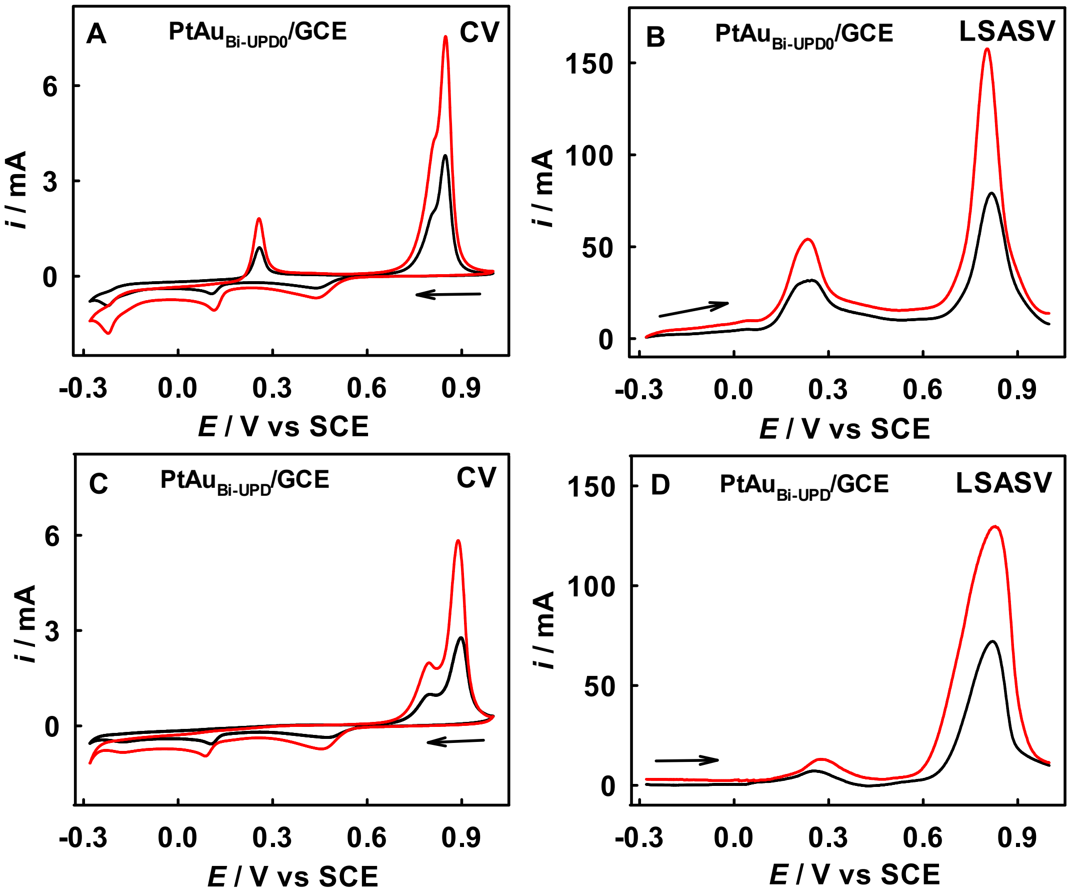

Fig. S7. CV curves on GCE in $PtAu_{Bi-UPD0}$ solution (A) or $PtAu_{Bi-UPD}$ solution (C). scan rate: 50 mV s^{-1}. LSASV on GCE after electrodeposition in $PtAu_{Bi-UPD0}$ solution (B) or $PtAu_{Bi-UPD}$ solution (D) at -0.28 V for 600 s. scan rate: 100 mV s^{-1}. The black lines show the $PtAu_{Bi-UPD0}$ or $PtAu_{Bi-UPD}$ original solution while the red lines show the $PtAu_{Bi-UPD0}$ or $PtAu_{Bi-UPD}$ original solution with adding standard solution. As shown in Fig. S7A and B, after dissolving some scraped $PtAu_{Bi-UPD0}$ with 40 μL aqua regia (V_{HCl}:V_{HNO3} = 3:1, highly corrosive, treat with great care), then adding 10 μL of 1 M aqueous HCl or 10 μL of 1 M aqueous HCl containing $PtCl_6^{2-}$, $AuCl_4^-$ and Bi(III) with known concentration (Table S1), followed by CV or LSASV characterizations on GCE. The reduction peaks at ca. 0.5 V, ca. 0.2 V and ca. -0.2 V can be assigned to the reduction of $AuCl_4^-$, $PtCl_6^{2-}$ and Bi(III) on GCE, respectively, and the oxidation peaks near ca. 0.25 V and ca. 0.85 V are due to the electrooxidation of Bi and Au.

As shown in Fig. S7C and D, after dissolving some scraped $PtAu_{Bi\text{-}UPD}$ with 40 μL aqua regia, then added 10 μL of 1 M aqueous HCl or 10 μL of 1 M aqueous HCl containing $PtCl_6^{2-}$, $AuCl_4^-$ and Bi(III) with known standard concentration (Table S1), followed by CV or LSASV characterizations on GCE. The reduction peaks at ca. 0.5 V, ca. 0.2 V and ca. -0.2 V can be assigned to the reduction of $AuCl_4^-$, $PtCl_6^{2-}$ on GCE and the reduction of oxygen at the active site of deposited gold, respectively, and the oxidation peaks near ca. 0.25 V and ca. 0.85 V are due to the electrooxidation of Bi and Au.

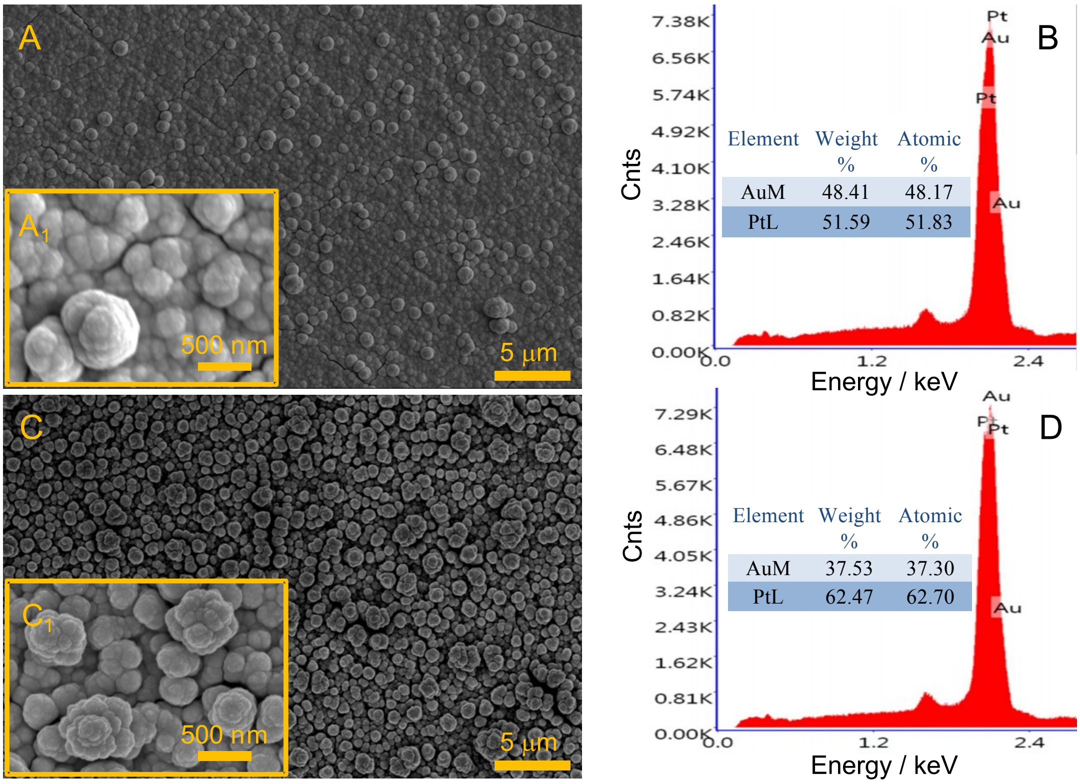

Element	Weight %	Atomic %
AuM	48.41	48.17
PtL	51.59	51.83

Element	Weight %	Atomic %
AuM	37.53	37.30
PtL	62.47	62.70

Fig. S8. SEM images and EDS spectra of PtAu$_{0V}$/GCE (A, A$_1$ and B) and PtAu$_{-0.04V}$/GCE (C, C$_1$ and D). Here, PtAu$_{0V}$/GCE and PtAu$_{-0.04V}$/GCE both show particles aggregation structure, and the corresponding EDS show typical energy peaks of Pt and Au elements, indicating that PtAu$_{0V}$/GCE and PtAu$_{-0.04V}$/GCE were successfully prepared.

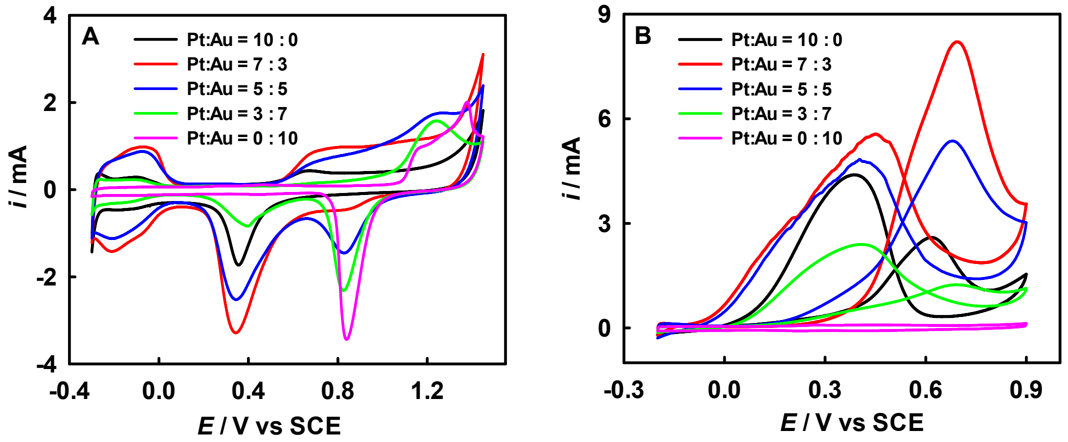

Fig. S9. CV curves on $Pt_{10}Au_{0\text{-Bi-UPD}}$/GCE, $Pt_7Au_{3\text{-Bi-UPD}}$/GCE, $Pt_5Au_{5\text{-Bi-UPD}}$/GCE, $Pt_3Au_{7\text{-Bi-UPD}}$/GCE, and $Pt_0Au_{10\text{-Bi-UPD}}$/GCE in 0.5 M aqueous H_2SO_4 (A) or 0.5 M H_2SO_4 + 0.1 M HCHO (B). Scan rate: 50 mV s^{-1}. Here, in order to improve the catalytic performance of $PtAu_{\text{Bi-UPD}}$/GCE, we optimized the concentration ratio of H_2PtCl_6 and $HAuCl_4$ in the electrodeposition solution. As shown in Fig. S9, the molar concentration ratio of H_2PtCl_6 and $HAuCl_4$ of 7:3 gave the largest electroactive area of Pt and the largest electrocatalytic response, thus 7:3 is chosen as the molar concentration ratio of H_2PtCl_6 and $HAuCl_4$.

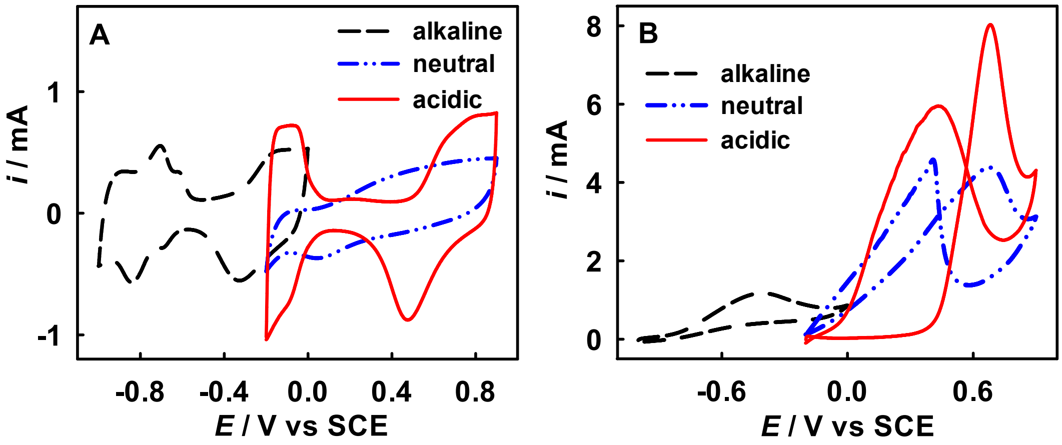

Fig. S10. (A) CV curves on PtAu$_{Bi\text{-}UPD}$/GCE in 0.1 M aqueous KOH (---), 0.1 M pH 7.0 aqueous Na_2SO_4 (-···-) or 0.5 M aqueous H_2SO_4 (¾). (B) CV curves on PtAu$_{Bi\text{-}UPD}$/GCE in 0.1 M KOH + 0.1 M HCHO (a), 0.1 M pH 7.0 Na_2SO_4 + 0.1 M HCHO (b) or 0.5 M H_2SO_4 + 0.1 M HCHO (c). Scan rate: 50 mV s^{-1}. Here, we studied the electrocatalytic oxidation of HCHO on PtAu$_{Bi\text{-}UPD}$/GCE in different pH solution. As shown in Fig. S10, the peak current of formaldehyde oxidation increased with the increase of solution acidity, and the peak of formaldehyde oxidation shifted to the right with the increase of solution acidity. From the view of thermodynamics, formaldehyde oxidation is a proton-coupled electron transfer process, and the alkaline solution is more conducive to formaldehyde oxidation. Therefore, the larger catalytic oxidation current of formaldehyde in acidic solution should indicate that the catalytic oxidation process of formaldehyde is mainly affected by kinetic factors. In summary, the electrocatalytic oxidation and detection of formaldehyde were carried out in 0.5 M aqueous H_2SO_4 later.

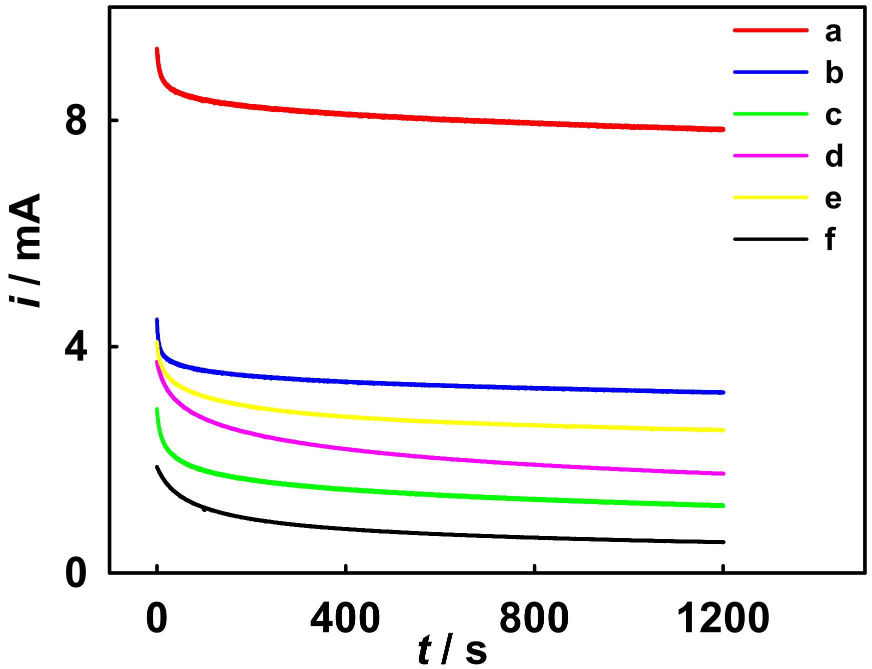

Fig. S11. Chronoamperometric curves of $PtAu_{Bi\text{-}UPD}$/GCE (a), $PtAu_{Bi\text{-}BD}$/GCE (b), $PtAu_{0V}$/GCE (c), $PtAu_{-0.04V}$/GCE (d) $Pt_{Bi\text{-}UPD}$/GCE (e) and Pt/C/GCE (f) in stirred aqueous solution of 0.5 M H_2SO_4 + 0.1M HCHO. Applied potential: 0.7 V vs. SCE. Here, according to the obtained chronoamperogram shown in Fig. S11, we calculate the long-term poisoning rate (δ, % s^{-1}) by measuring the linear attenuation of the current after 500 s[15], $\delta=(100/I_0)\times(dI/dt)_{t>500s}$, where $(dI/dt)_{t>500s}$ is the slope of the linear portion of the current decay and I_0 is the current at the start of polarization back extrapolated from the linear current decay. The δ value follows the order $PtAu_{Bi\text{-}UPD}$/GCE (0.005% s^{-1}) < $PtAu_{Bi\text{-}BD}$/GCE (0.01% s^{-1}) < $Pt_{Bi\text{-}UPD}$/GCE (0.015% s^{-1}) < $PtAu_{0V}$/GCE (0.02% s^{-1}) < $PtAu_{-0.04V}$/GCE (0.025% s^{-1}) < /Pt/C/Au_{pla}/GCE (0.03% s^{-1}), quantitatively indicating the highest stability of $PtAu_{Bi\text{-}UPD}$/GCE. The current loss on $PtAu_{Bi\text{-}UPD}$/GCE is partially due to the anticipated depletion of the reactant, electrooxidation of Au may be not so obvious at this potential in this acidic medium, and anodic dissolution of remaining Bi species may be difficult due to the residue of electrolyte-inaccessible internal Bi atoms (enveloped by Pt and Au atoms).

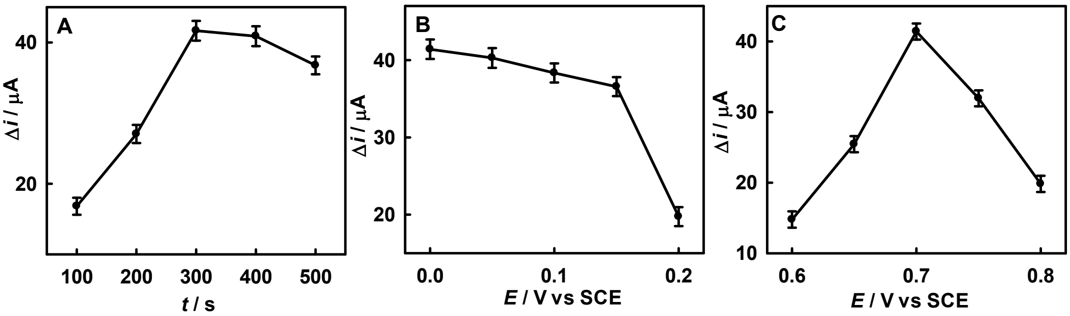

Fig. S12. Optimization of underpotential/bulk codeposition time (A), UPD potential (B) and detection potential (C) for PtAu$_{\mathrm{Bi\text{-}UPD}}$/GCE. The response currents for 0.2 mM HCHO (Δ*i*) were obtained in 0.5 M H_2SO_4 solution. Parameters: underpotential/bulk codeposition time = 300 s, UPD potential = 0 V and detection potential = 0.7 V, except the parameter under optimization. Here, as shown in Fig. S12, the catalytic current response was almost stable at the highest value when the underpotential/bulk codeposition time was 300 s. The more negative deposition potential in the selected potential range is favorable for the greater catalytic current response, due to the specified UPD potentials. When the deposition potential was 0 V, the oxidation current response of PtAu$_{\mathrm{Bi\text{-}UPD}}$/GCE to HCHO was the best. The formaldehyde-sensing potential was optimized to 0.7 V, since a higher potential may yield notable Pt oxides against the catalysis, and 0.7 V is thus identified as the applied potential in the following chronoamperometry.

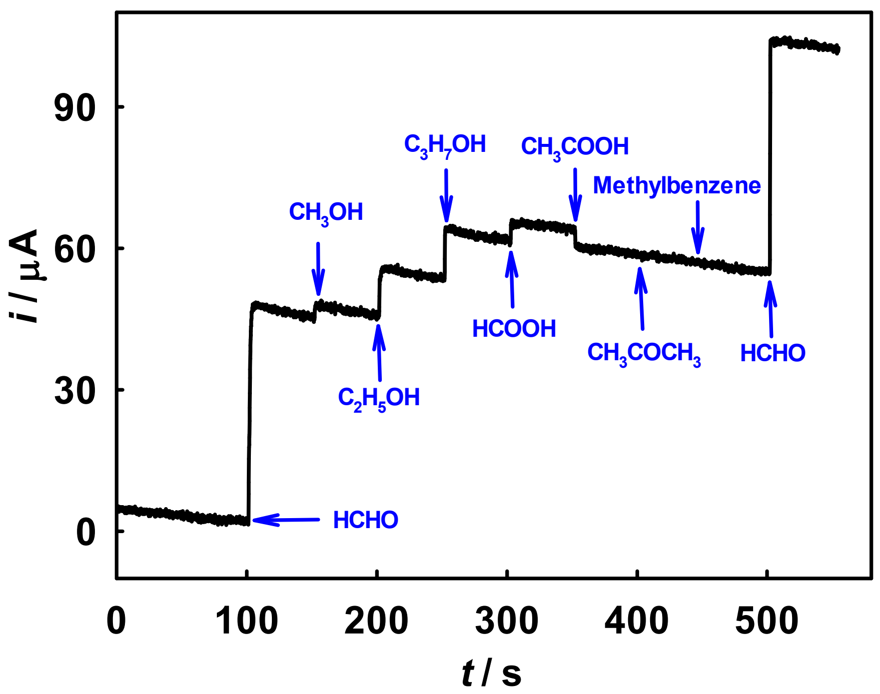

Fig. S13. Amperometric response of PtAu$_{Bi\text{-}UPD}$/GCE to the successive additions of 0.2 mM HCHO, 0.2 mM CH_3OH, 0.2 mM C_2H_5OH, 0.2 mM C_3H_7OH, 0.2 mM HCOOH, 0.2 mM CH_3COOH, 0.2 mM CH_3COCH_3, 0.2 mM methylbenzene, and 0.2 mM HCHO into stirred 0.5 M aqueous H_2SO_4 at 0.7 V vs SCE. Here, to evaluate the selectivity of PtAu$_{Bi\text{-}UPD}$/GCE, possible interfering substances (formic acid, acetic acid, methanol, ethanol, propanol, acetone or toluene) were investigated. PtAu$_{Bi\text{-}UPD}$/GCE is sensitive to formaldehyde detection, but has low current response to low-concentration formic acid, acetic acid, methanol, ethanol or propanol, and no current response to low-concentration acetone and toluene. This observation shows that PtAu$_{Bi\text{-}UPD}$/GCE has good selectivity for formaldehyde detection.

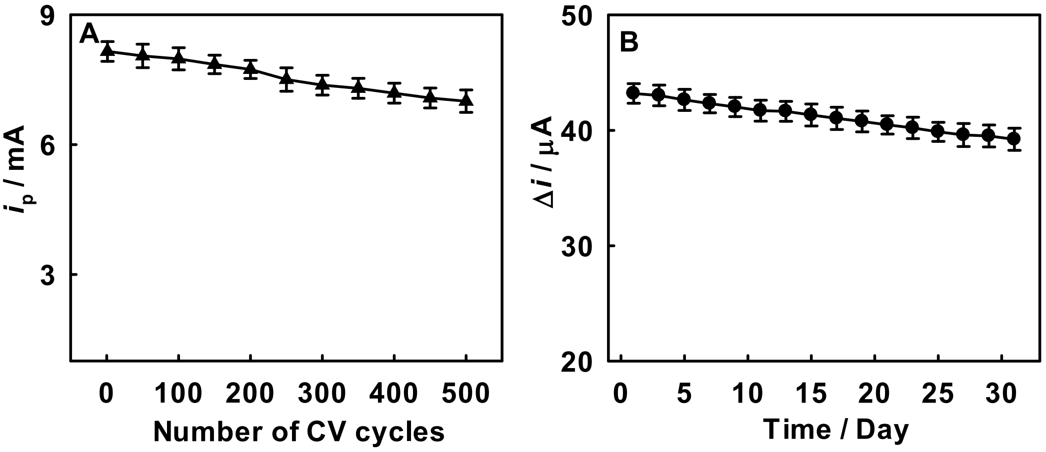

Fig. S14. (A) The attenuation of oxidation peak current with the number of potential cycles on PtAu$_{Bi\text{-}UPD}$/GCE in 0.5 M H_2SO_4 + 0.1 M HCHO. Scan rate: 50 mV s^{-1}. (B) Long-time stability of PtAu$_{Bi\text{-}UPD}$/GCE to 0.5 M H_2SO_4 + 0.2 mM HCHO. Applied potential: 0.7 V. Here, we evaluated the stability of catalytic oxidation of formaldehyde on PtAu$_{Bi\text{-}UPD}$/GCE by continuous potential cycling. As shown in Fig. S14A, after continuous 200 cycles, the CV peak current response of PtAu$_{Bi\text{-}UPD}$/GCE to 0.1 M HCHO still retained 95% of the initial value. The current response dropped to 86% of the initial value after 500 cycles. As shown in Fig. S14B, the storage stability of the PtAu$_{Bi\text{-}UPD}$/GCE was tested with the catalytic current response in aqueous 0.2 mM HCHO + 0.5 M H_2SO_4 as the quantitative indexes over a period of 30 days. The current response still retained 91% of the initial value after 30 days.

References (The numbering here is only for the ESI)

1 L. Chao, N. Liu, X. Xiong, F. He, T. Huang, Q. Xie and S. Yao, *Chem. Commun.*, 2018, **54**, 3743.

2 H. Mei, W. Wu, B. Yu, H. Wu, S. Wang and Q. Xia, *Sens. Actuators B: Chem*., 2016, **223**, 68.

3 F. Xiao, F. Zhao, L. Deng and B. Zeng, *Electrochem. Commun.*, 2010, **12**, 620.

4 O. Demkiv, O. Smutok, M. Gonchar and M. Nisnevitch*, Materials*, 2017, **10**, 503.

5 Y. Chen, X. Liu, W. Zhang, Y. Zhang, L. Li, Z. Cao, H. Wang, G. Jia, Y. Gao and J. Liu, *Anal. Methods*, 2013, **5**, 3915.

6 Z. L. Zhou, T. F. Kang, Y. Zhang and S. Y. Cheng, *Microchim. Acta*, 2009, 164, 133.

7 M. R. Mahmoudian, W. J. Basirun, P. M. Woi, H. Hazarkhani and Y. B. Alias, *Microchim. Acta*, 2019, **186**, 1.

8 Y. Zhang, M. Zhang, Z. Cai, M. Chen and F. Cheng, *Electrochim. Acta*, 2012, **68**, 172.

9 Q. Wang, J. Zheng and H. Zhang, *J. Electroanal. Chem.*, 2012, **674**, 1.

10 Q. Yi, F. Niu and W. Yu, *Thin Solid Films*, 2011, **519**, 3155.

11 H. Xi, X. Chen, Y. Cao, J. Xu, C. Ye, D. Deng, J. Zhang and G. Huang, *Microchem. J.*, 2020, **156**, 104846.

12 W. Yuan, J. Zhang, P. K. Shen, C. M. Li and S. P. Jiang, *Electrochim. Acta*, 2016, **190**, 817.

13 Z. Xi, H. Lv, D. P. Erdosy, D. Su, Q. Li, C. Yu and J. Li, S. Sun, *Nanoscale*, 2017, **9**, 7745.

14 S. H. Zheng, K. Krug, F. Golks, D. Kaminski, S. Morin and O. M. Magnussen, *J. Electroanal. Chem*., 2010, **649**, 189.

15 J. W. Guo, T. S. Zhao, J. Prabhuram, R. Chen and C. W. Wong, *J. Power Sources*, 2006, **156**, 345.